

Planar Bipedal Walking with Anthropomorphic Foot Action

Jun Ho Choi, *Student Member, IEEE*, and J.W. Grizzle, *Fellow, IEEE*

Abstract—This paper investigates the key problem of walking with both fully actuated and underactuated phases. The studied robot is planar, bipedal, and fully actuated in the sense that it has feet with revolutes, actuated ankles. The desired walking motion is assumed to consist of three successive phases: a fully-actuated phase where the stance foot is flat on the ground, an underactuated phase where the stance heel lifts from the ground and the stance foot rotates about the toe, and an instantaneous double support phase where leg exchange takes place. The main contribution of the paper is to provide a provably asymptotically stabilizing controller that integrates the fully-actuated and underactuated phases of walking. By comparison, existing humanoid robots, such as Asimo and Qrio, use only the fully-actuated phase (i.e., they only execute flat-footed walking), or RABBIT, which uses only the underactuated phase (i.e., it has no feet, and hence walks as if on stilts). The controller proposed here is organized around the hybrid zero dynamics of Westervelt *et al.* (2003) in order that the stability analysis of the closed-loop system may be reduced to a one-dimensional Poincaré map that can be computed in closed form. The ubiquitous Zero Moment Point (ZMP) is used to establish conditions under which the foot will not rotate about its extremities; the ZMP is not used for stability analysis. An example is given to show that a periodic walking motion can be unstable while the ZMP remains strictly within the footprint of the robot.

Index Terms—Robotics; Humanoids; Hybrid Zero Dynamics; Orbital Stability; Poincaré map; ZMP.

I. INTRODUCTION

THE stance foot plays an important role in human walking since it contributes to forward progression, vertical support, and initiation of the lifting of the swing leg from the ground [1], [2]. This paper addresses the modeling and control of planar bipedal robots with feet, with emphasis on a walking motion that allows anthropomorphic foot action [3] as depicted in Figure 1. The associated model is hybrid in nature, with phases modeled by ordinary differential equations interleaved with discrete transitions and reset maps. Furthermore, one of the phases is underactuated. Stable walking corresponds to the design of asymptotically stable periodic orbits in these hybrid systems and not equilibrium points. Feedback laws are proposed to create periodic orbits and their stability properties are established through a careful analysis of the Poincaré return map. This is quite different than the prevailing methods in the controlled-biped literature where heuristic stability criteria are commonly used.

Over the past decade, several remarkably anthropomorphic robots have been constructed, such as the well known

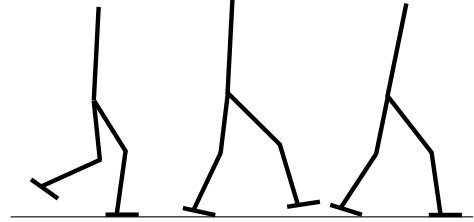


Fig. 1. The three phases of walking modeled in this paper: fully-actuated phase where the stance foot is flat on the ground, underactuated phase where the stance heel rises from the ground and the stance foot rotates about the stance toe, and double-support phase where the swing foot impacts the ground.

Honda Robot, Asimo [4], [5], Sony’s biped, Qrio [6], and Johnnie at the University of Munich [7], [8]. Each of these robot’s control systems is organized around a high-level trajectory generator for the individual joints of the robot, combined with low-level servoing to ensure trajectory tracking. There are some differences in how the low-level servoing is implemented—Honda uses PD control [5], Johnnie uses feedback linearization [8], while Sony has revealed little about their algorithms—but these differences are fairly insignificant. In each case, the overall “stability” of the robot’s motion has been based on the Zero Moment Point (ZMP) criterion (see Figure 2), and consequently, these robots literally walk flat footed.

A stability analysis of a flat-footed walking gait for a five-link biped with an actuated ankle was carried out numerically in [9], [10], using the Poincaré return map. The control law used feedback linearization to maintain the robot’s posture and advance the swing leg; trajectory tracking was only used in the limited sense that the horizontal component of the center of mass was commanded to advance at a constant rate. The unilateral constraints due to foot contact were carefully presented. Motivated by energy efficiency, elegant work in [11], [12] has shown how to realize a passive walking gait in a fully actuated biped robot walking on a flat surface. Stability of the resulting walking motion has been rigorously established. The main drawback, however, is that the assumption of full actuation once again restricts the foot motion to flat-footed walking.

For walking gaits that include foot rotation, various *ad hoc* control solutions have been proposed in the literature [14], [15], [16], [17], [18], [19], but none of them can guarantee stability in the presence of the underactuation that occurs during heel roll or toe roll. Our previous work on point feet [20], [21], [22], [23], [24] ideally positions us to handle this underactuation; indeed, conceptually, a point foot corresponds to continuous rotation about the toe throughout the entire stance phase (e.g., walking like a ballerina or as if on stilts).

This work was supported by NSF grant ECS-0322395.

Jun Ho Choi is with the Intelligent Robotics Research Center, Korea Institute of Science and Technology, Hawolgok-dong 39-1, Sungbuk-ku, Seoul 136-791, Korea, junhochoi@kist.re.kr

J. W. Grizzle is with the Department of Electrical Engineering and Computer Science, University of Michigan, Ann Arbor, Michigan 48109-2122, USA, grizzle@umich.edu

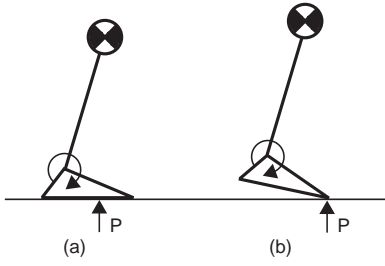


Fig. 2. The ZMP (Zero Moment Point) principle in a nutshell. Idealize a robot in single support as a planar inverted pendulum attached to a base consisting of a foot with torque applied at the ankle and all other joints are independently actuated. Assume adequate friction so that the foot is not sliding. In (a), the robot's nominal trajectory has been planned so that the center of pressure of the forces on the foot, P , remains strictly within the interior of the footprint. In this case, the foot will not rotate (i.e., the foot is acting as a base, as in a normal robotic manipulator), and thus the system is fully actuated. It follows that small deviations from the planned trajectory can be attenuated via feedback control. In case (b), however, the center of pressure has moved to the toe, allowing the foot to rotate. The system is now underactuated (two degrees of freedom and one actuator), and designing a stabilizing controller is nontrivial, especially when impact events are taken into account. The ZMP principle says to design trajectories so that case (a) holds; i.e., walk flat footed. Humans, even with prosthetic legs, use foot rotation to decrease energy loss at impact [13].

Work in [13] shows that plantarflexion of the ankle, which initiates heel rise and toe roll, is the most efficient method to reduce energy loss at the subsequent impact of the swing leg. This motion is also necessary for the *esthetics* of mechanical walking.

In this paper, the analysis of walking with point feet is extended to design a controller that provides asymptotically stable walking with an anthropomorphic foot motion¹. In particular, Section II models a walking motion consisting of three successive phases²: a fully-actuated phase where the stance foot is flat on the ground, an underactuated phase where the stance heel lifts from the ground and the stance foot rotates about the toe, and an instantaneous double-support phase where leg exchange takes place, see once again Figure 1. A control law is proposed in Sections III and IV, based on virtual constraints. The hybrid zero dynamics is used to reduce the complexity of the associated stability analysis problem. A systematic method for choosing the virtual constraints is given in Section V, with an illustrative example worked out in Section VI. In Section VII, flat-footed walking is recovered as a special case of the results of Section III. In order to underline that the ZMP principle alone is not sufficient for the stability of a walking gait, this result is used in Section VIII to construct a periodic orbit on which the ZMP principle is satisfied at each point of the gait, but yet the orbit is unstable. Conclusions are given in Section IX.

II. ROBOT MODEL

The robot considered in this paper is bipedal and planar with $N \geq 4$ rigid links connected by ideal (frictionless) revolute joints to form a tree structure (no closed kinematic chains). It is assumed to have two identical open chains called

¹A summary of this work was reported in [25].

²For simplicity, heel strike with a subsequent heel roll is not addressed. It can be handled in the same manner as toe roll.

“legs” that are connected at a point called the “hips.” The link at the extremity of each leg is called a “foot” and the joint between the foot and the remainder of the leg is called an “ankle.” The feet are assumed to be “forward facing.” The forward end of each foot is called a “toe” and the back end is called a “heel.” Each revolute joint is assumed to be independently actuated. It is assumed that walking consists of three successive phases, a fully-actuated phase, an underactuated phase, and a double-support phase, see Figure 1. The detailed assumptions for the robot and the gait are listed in Appendix I. A representative robot is shown in Figure 3 along with a coordinate convention.

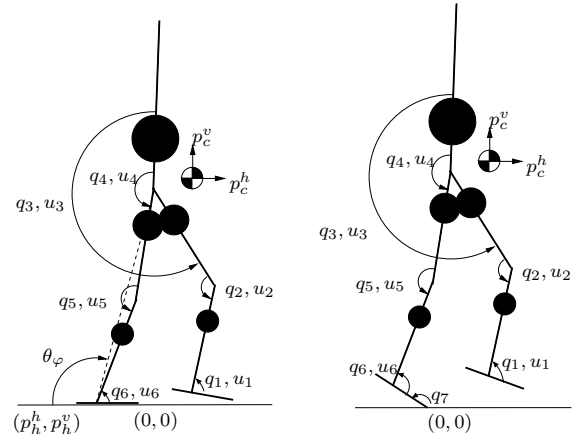


Fig. 3. Model of a 7-link robot with coordinate convention. θ_v is not shown. It is defined as $\theta_v = \pi - q_7 + \theta_\varphi$. In general, for an N -link robot, it is assumed that q_{N-1} is the angle between the stance foot and the stance tibia and q_N is the angle between the ground and the stance foot.

A. Underactuated phase

The underactuated phase is when the stance heel of the robot rises from the ground and the robot begins to roll over the stance toe; this condition is characterized by the foot rotation indicator (FRI) point of [26] being strictly in front of the stance foot. The stance toe is assumed to act as a pivot; this condition is characterized by the forces at the toe lying within the allowed friction cone. Both of these conditions (i.e., foot rotation and non-slip) are constraints that must be imposed in the final controller design phase, which is discussed in Section V.

Since there is no actuation between the stance toe and the ground, the dynamics of the robot in this phase is equivalent to an N -DOF robot with unactuated point feet and identical legs, as treated in [21]. Define the generalized coordinates as $q_v = (q_1, \dots, q_N)^\top \in \mathcal{Q}_v$, where \mathcal{Q}_v is a simply connected open subset of \mathbb{R}^N . The dynamics are obtained using the method of Lagrange, yielding

$$D_v(q_v)\ddot{q}_v + C_v(q_v, \dot{q}_v)\dot{q}_v + G_v(q_v) = B_v u_v, \quad (1)$$

where $u_v = (u_1, \dots, u_{N-1})^\top$ is the vector of torques applied at the joints. The dynamic equation in state-variable form is expressed as $\dot{x}_v = f_v(x_v) + g_v(x_v)u_v$.

B. Fully-actuated phase

During the fully-actuated phase, the stance foot is assumed to remain flat on the ground without slipping. The ankle of the stance leg is assumed to act as an actuated pivot. Since the stance foot is motionless during this phase, the dynamics of the robot during the fully-actuated phase is equivalent to an $N - 1$ DOF robot without the stance foot and with actuation at the stance ankle, as studied in [27]. Let $q_\varphi = (q_1, \dots, q_{N-1})^\top \in \mathcal{Q}_\varphi$ be the configuration variables, where q_1, \dots, q_{N-2} denote the relative angles of the joints except the stance ankle, q_{N-1} denotes the angle of the stance ankle joint, and \mathcal{Q}_φ is a simply connected open subset of \mathbb{R}^{N-1} , see Figure 3. Note that because the stance foot remains on the ground, q_{N-1} is now an absolute angle (i.e., it is referenced to the world frame).

The dynamics for the fully-actuated phase are derived using the method of Lagrange, yielding a model of the form

$$D_\varphi(q_\varphi)\ddot{q}_\varphi + C_\varphi(q_\varphi, \dot{q}_\varphi)\dot{q}_\varphi + G_\varphi(q_\varphi) = B_{\varphi 1}u_b + B_{\varphi 2}u_A, \quad (2)$$

where \dot{q}_φ are the velocities, $u_A = u_{N-1}$ is the input at the ankle joint, and $u_b = (u_1, \dots, u_{N-2})^\top$ are the inputs applied at the remaining joints. The state is taken as $x_\varphi = (q_\varphi; \dot{q}_\varphi) \in T\mathcal{Q}_\varphi$ and the dynamic equation is given by³

$$\begin{aligned} \dot{x}_\varphi &= \begin{bmatrix} \dot{q}_\varphi \\ D_\varphi^{-1}(-C_\varphi\dot{q}_\varphi - G_\varphi + B_{\varphi 2}u_A) \end{bmatrix} + \begin{bmatrix} 0 \\ D_\varphi^{-1}B_{\varphi 1}u_b \end{bmatrix} \\ &=: f_\varphi(x_\varphi, u_A) + g_\varphi(x_\varphi)u_b. \end{aligned} \quad (3)$$

Note that, to satisfy the condition that the stance foot is flat on the ground, the FRI point needs to be kept strictly within the support region of the foot. This constraint must be imposed in the final controller design stage, see Section V.

C. Double-support phase

During the double-support phase, the swing foot impacts the ground. For simplicity, it is assumed that the swing foot is parallel to the ground at impact. It is also assumed that the feet are arc shaped so that the only contact points with the ground are the heel and the toe, see Figure 4. Due to



Fig. 4. Examples of feet. As long as the toe and heel are the only contact points with the ground, (a) and (b) are equivalent.

the impacts, impulsive forces are applied at the toe and the heel simultaneously, which cause discontinuous changes in the velocities; however, the position states are assumed to remain continuous [28]; the full set of hypotheses is listed in Appendix I.

Representing the double-support phase requires an $N+2$ DOF model (e.g. N DOF for the joints and 2 DOF for the position of the center of mass). Adding Cartesian coordinates,

³Note that the ankle torque is included in $f_\varphi(x_\varphi, u_A)$; the reason for this will be clear in Section III.

(p_c^h, p_c^v) , to the center of mass of the robot gives $q_d = (q_v; p_c^h; p_c^v)$ and $\dot{q}_d = (\dot{q}_v; \dot{p}_c^h; \dot{p}_c^v)$, see Figure 3. Since the swing heel and the swing toe are assumed to land on the ground at the same time, there are two ground reaction forces, which can be modeled as a resultant force and torque at the swing ankle. Let $\Upsilon_a^F(q_d)$ denote the Cartesian coordinates of the swing ankle and let $\Upsilon_a^\tau(q_d)$ denote the absolute angle of the swing foot. The method of Lagrange yields the dynamics for the double-support phase as follows:

$$\begin{aligned} D_d(q_d)\ddot{q}_d + C_d(q_d, \dot{q}_d)\dot{q}_d + G_d(q_d) \\ = B_d u + E_d^F \delta F + E_d^\tau \delta \tau, \end{aligned} \quad (4)$$

where $u = (u_b; u_A)$, $E_d^F = \left(\frac{\partial \Upsilon_a^F(q_d)}{\partial q_d} \right)^\top$, $E_d^\tau = \left(\frac{\partial \Upsilon_a^\tau(q_d)}{\partial q_d} \right)^\top$, and δF and $\delta \tau$ denote the resultant ground reaction force and the torque at the swing ankle, respectively.

Under the hypotheses IH6 (the actuators not being impulsive) and IH1 (which is the stance foot neither rebounds nor slips), following the procedure in [20] gives

$$\begin{aligned} x_\varphi^+ &= \begin{bmatrix} [R \ 0] q_d^- \\ [R \ 0] \Pi \begin{bmatrix} D_d \dot{q}_d^- \\ 0 \end{bmatrix} \end{bmatrix} \\ &= \begin{bmatrix} \Delta_{q,v}^\varphi(q_v^-) \\ \Delta_{\dot{q},v}^\varphi(q_v^-) \dot{q}_v^- \end{bmatrix} := \Delta_v^\varphi(x_d^-), \end{aligned} \quad (5)$$

where R is a relabeling matrix and

$$\Pi = \begin{bmatrix} D_d & -E_d^F & -E_d^\tau \\ (E_d^F)^\top & 0 & 0 \\ (E_d^\tau)^\top & 0 & 0 \end{bmatrix}^{-1}. \quad (6)$$

Note that, because the stance toe acts as a pivot just before the impact, x_d^- is uniquely determined by x_v^- .

D. Foot Rotation, or Transition from Full Actuation to Underactuation

The transition from a flat foot to rotation about the toe can be initiated by causing the angular acceleration about the stance toe to become negative. To characterize the motion of the stance foot, or equivalently, when the robot transitions from full actuation—foot is flat on the ground—to underactuation—foot rotates about the toe, the foot rotation indicator (FRI) point of Goswami is used [26]. See Appendix II for the detailed calculation.

By enforcing that the FRI point is strictly in front of the stance foot, the transition is initiated. If torque discontinuities⁴ are allowed—as they are assumed to be in this paper—when to allow foot rotation becomes a control decision. Here, in view of simplifying the analysis of periodic orbits in Section IV, the transition is assumed to occur at a fixed point in the fully-actuated phase⁵. Hence, $H_\varphi^v = \theta_\varphi(q_\varphi) - \theta_{\varphi,0}^-$, where $\theta_\varphi(q_\varphi)$ is the angle of the hips with respect to the stance ankle (see Figure 3) and $\theta_{\varphi,0}^-$ is a constant to be determined.

⁴This is a modeling decision. In practice, the torque is continuous due to actuator dynamics. It is assumed here that the actuator time constant is small enough that it need not be modeled.

⁵When the transition condition is met, namely, $\theta_\varphi = \theta_{\varphi,0}^-$, a jump in the torque is made to achieve $\dot{q}_N < 0$. This moves the FRI point in front of the foot.

The positions and the velocities remain continuous with a step-change in torque. The ensuing initial value of the underactuated phase, x_v^+ , is defined so as to achieve continuity in the position and velocity variables:

$$x_v^+ = \begin{bmatrix} q_v^+ \\ \dot{q}_v^+ \end{bmatrix} = \begin{bmatrix} q_\varphi^- \\ \pi \\ \dot{q}_\varphi^- \\ 0 \end{bmatrix} =: \Delta_\varphi^v(x_\varphi^-). \quad (7)$$

Continuity of the torques is not imposed, and hence neither is continuity of the accelerations. It is assumed that the control law in the underactuated phase will be designed so that the FRI point is in front of the toe.

E. Overall Hybrid Model

As in [29], the overall model can be expressed as a nonlinear hybrid system containing two state manifolds (called “charts” in [30]):

$$\Sigma_\varphi : \begin{cases} \mathcal{X}_\varphi &= T\mathcal{Q}_\varphi \\ \mathcal{F}_\varphi : \dot{x}_\varphi &= f_\varphi(x_\varphi, u_A) + g_\varphi(x_\varphi)u_b \\ \mathcal{S}_\varphi^v &= \{x_\varphi \in T\mathcal{Q}_\varphi | H_\varphi^v(x_\varphi) = 0\} \\ \mathcal{T}_\varphi^v : x_v^+ &= \Delta_\varphi^v(x_\varphi^-) \end{cases} \quad (8)$$

$$\Sigma_v : \begin{cases} \mathcal{X}_v &= T\mathcal{Q}_v \\ \mathcal{F}_v : \dot{x}_v &= f_v(x_v) + g_v(x_v)u_v \\ \mathcal{S}_v^\varphi &= \{x_v \in T\mathcal{Q}_v | H_v^\varphi(x_v) = 0\} \\ \mathcal{T}_v^\varphi : x_\varphi^+ &= \Delta_v^\varphi(x_v^-) \end{cases}$$

where, for example, \mathcal{F}_φ is the flow on state manifold \mathcal{X}_φ , \mathcal{S}_φ^v is the switching hyper-surface for transitions between \mathcal{X}_φ and \mathcal{X}_v , $\mathcal{T}_\varphi^v : \mathcal{S}_\varphi^v \rightarrow \mathcal{X}_v$ is the transition function applied when $x_\varphi \in \mathcal{S}_\varphi^v$.

The transition from the underactuated phase to the fully-actuated phase occurs when the swing foot impacts the ground. Hence, $H_\varphi^v(x_v) = \Upsilon_h^v(x_v)$, where $\Upsilon_h^v(x_v)$ denotes the vertical coordinate (height) of the swing heel, see Figure 5.

Remark 1: \mathcal{S}_φ^v is read as the switching surface **from** the fully-actuated phase, φ , **to** the underactuated phase denoted v .

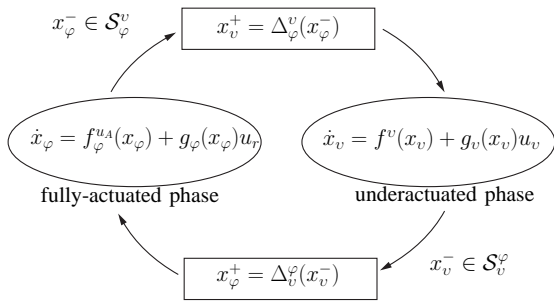


Fig. 5. Diagram of system.

III. CREATING THE HYBRID ZERO DYNAMICS

In a certain sense, the basic idea of the control law design is quite straightforward. Following the development in [21],

[23], we use the method of virtual constraints to create a two-dimensional zero dynamics manifold \mathcal{Z}_v in the $2N$ -dimensional state space of the underactuated phase. This requires the use of the full complement of $N - 1$ actuators on the robot. In the fully-actuated phase, we have one less degree of freedom because the stance foot is motionless and flat on the ground. Consequently, we use $N - 2$ actuators—all actuators except the ankle of the stance foot—to create a two-dimensional zero dynamics manifold \mathcal{Z}_φ —that is compatible with \mathcal{Z}_v in the sense that the following invariance conditions hold: $\Delta_\varphi^v(\mathcal{S}_\varphi^v \cap \mathcal{Z}_\varphi) \subset \mathcal{Z}_v$ and $\Delta_v^\varphi(\mathcal{S}_v^\varphi \cap \mathcal{Z}_v) \subset \mathcal{Z}_\varphi$. The actuation authority at the ankle is subsequently employed for stability and efficiency augmentation, and for enforcing the non-rotation of the foot. The invariance conditions guarantee the existence of a hybrid zero dynamics for the closed-loop hybrid model. The techniques in [21] are then extended to compute the Poincaré map of the closed-loop system in closed form. Precise stability conditions then follow.

A. Control design for the underactuated phase

The greatest difficulties in the control design and analysis involve the underactuated phase of the motion. Since the stance toe acts as a pivot and there is no actuation at the stance toe, the feedback design proceeds as in [21]. Let $y_v = h_v(x_v)$ be an $(N - 1) \times 1$ vector of output functions satisfying the following hypotheses:

HHU1) The output function $h_v(x_v)$ depends only on the configuration variables;

HHU2) The decoupling matrix $L_{g_v}L_{f_v}h_v$ is invertible for an open set $\tilde{\mathcal{Q}}_v \subset \mathcal{Q}_v$;

HHU3) Existence of $\theta_v(q_v)$ such that $[h_v(q_v); \theta_v(q_v)]$ is a diffeomorphism;

HHU4) There exists a point in $\tilde{\mathcal{Q}}_v$ where h_v vanishes.

HHU5) There exists a unique point $q_{v,0}^- \in \tilde{\mathcal{Q}}_v$ such that $(h_v(q_{v,0}^-), \Upsilon_a^v(q_{v,0}^-)) = (0, 0)$, $\Upsilon_t^h(q_{v,0}^-) > 0$ and the rank of $[h_v; \Upsilon_a^v]$ at $q_{v,0}^-$ equals to N , where $\Upsilon_t^h(x_v)$ denotes the horizontal coordinate of the swing toe.

Then there exists a smooth manifold $\mathcal{Z}_v = \{x_v \in T\mathcal{Q}_v | h_v(x_v) = 0, L_{f_v}h_v(x_v) = 0\}$, called the underactuated-phase zero dynamics manifold, and $\mathcal{S}_\varphi^v \cap \mathcal{Z}_v$ is smooth. $\mathcal{S}_\varphi^v \cap \mathcal{Z}_v$ is one-dimensional if $\mathcal{S}_\varphi^v \cap \mathcal{Z}_v \neq \emptyset$. Differentiating the output y_v twice yields,

$$\ddot{y}_v = \nu_v \quad (9)$$

$$= L_{f_v}^2 h_v(x_v) + L_{g_v}L_{f_v}h_v(x_v)u_v. \quad (10)$$

Since the decoupling matrix $L_{g_v}L_{f_v}h_v(x_v)$ is invertible, the feedback control

$$u_v^* := -(L_{g_v}L_{f_v}h_v(x_v))^{-1}(L_{f_v}^2 h_v(x_v)) \quad (11)$$

renders the zero dynamics manifold invariant. In addition to the hypotheses HHU1–HHU5, if hypothesis RH5 in the Appendix I is also satisfied, then the underactuated phase zero dynamics in the coordinates of $z_v := (\theta_v, \sigma_v) = (\theta_v, d_v(q_v)\dot{q}_v)$ can be written as

$$\dot{\theta}_v = \kappa_v^1(\theta_v)\sigma_v \quad (12)$$

$$\dot{\sigma}_v = \kappa_v^2(\theta_v), \quad (13)$$

where d_v is the last row of D_v and σ_v is the angular momentum about the stance toe during the underactuated phase, [31]. Equations (12) and (13) are written as $\dot{z}_v = f_{\mathcal{Z}_v}(z_v)$.

The transition map from the underactuated phase to the fully-actuated phase on the hybrid zero dynamics becomes

$$\theta_\varphi^+ = \theta_\varphi \circ [R \ 0] q_v^-, \quad (14)$$

$$\sigma_\varphi^+ = \delta_\varphi^\varphi \sigma_v^-, \quad (15)$$

where δ_φ^φ is a constant that can be calculated as in [21].

B. Control design for the fully-actuated phase

Since the stance foot is motionless and acting as a base during this phase, the model only has $N - 1$ DOF. Consequently, the robot is fully actuated, opening up many feedback design possibilities. For example, we could, in principle, design for an empty zero dynamics, feedback linearize the model, etc. —*though we would run a high risk of requiring so much ankle torque that the foot would rotate, thereby causing underactuation*. Instead, we follow a design where, in principle, the ankle torque could be used exclusively for ensuring that the foot does not rotate, but in most cases, it can also be used to augment stability and efficiency of the overall walking cycle.

$N - 2$ virtual constraints are used to create a two-dimensional zero dynamics for the fully-actuated phase that is driven by the ankle torque. Let $y_\varphi = h_\varphi(x_\varphi)$ be a $(N - 2) \times 1$ vector of output functions. Let the output function y_φ satisfy the following hypotheses:

HHF1) The output function $h_\varphi(x_\varphi)$ depends only on the configuration variables of the fully-actuated phase;

HHF2) For $u_A = 0$, the decoupling matrix $L_{g_\varphi} L_{f_\varphi} h_\varphi$ is invertible for an open set $\tilde{\mathcal{Q}}_\varphi \subset \mathcal{Q}_\varphi$;

HHF3) There exists $\theta_\varphi(q_\varphi)$ such that $[h_\varphi(q_\varphi); \theta_\varphi(q_\varphi)]$ is a diffeomorphism;

HHF4) There exists a point where h_φ vanishes;

HHF5) There exists a unique point $q_{\varphi,0}^- \in \tilde{\mathcal{Q}}_\varphi$ such that $y_\varphi = h_\varphi(q_{\varphi,0}^-) = 0$, $H_\varphi^v(q_{\varphi,0}^-) = 0$ and $[h_\varphi; H_\varphi^v]$ has full rank.

Then there exists a smooth manifold $\mathcal{Z}_\varphi = \{x_\varphi \in T\mathcal{Q}_\varphi | h_\varphi(x_\varphi) = 0, L_{f_\varphi} h_\varphi(x_\varphi) = 0\}$, called the fully-actuated-phase zero dynamics manifold, and $\mathcal{S}_\varphi^v \cap \mathcal{Z}_\varphi$ is smooth. $\mathcal{S}_\varphi^v \cap \mathcal{Z}_\varphi$ is one-dimensional if $\mathcal{S}_\varphi^v \cap \mathcal{Z}_\varphi \neq \emptyset$.

Differentiating twice the output y_φ for the fully-actuated phase gives

$$\ddot{y}_\varphi := \nu_\varphi \quad (16)$$

$$= L_{f_\varphi}^2 h_\varphi(x_\varphi) + L_{g_\varphi} L_{f_\varphi} h_\varphi(x_\varphi) u_b. \quad (17)$$

Since $L_{g_\varphi} L_{f_\varphi} h_\varphi$ is invertible, the feedback control

$$u_b^* = -(L_{g_\varphi} L_{f_\varphi} h_\varphi(x_\varphi))^{-1} (L_{f_\varphi}^2 h_\varphi(x_\varphi, u_A)) \quad (18)$$

renders the zero dynamics manifold for the fully-actuated phase invariant.

In addition to the hypotheses HHF1–HHF5, if the hypothesis RH5 is satisfied, then in the coordinates of $z_\varphi := (\theta_\varphi, \sigma_\varphi) = (\theta_\varphi, d_\varphi(q_\varphi)\dot{q}_\varphi)$ restricted to the zero dynamics

manifold, the fully-actuated phase zero dynamics can be written as

$$\dot{\theta}_\varphi = \kappa_\varphi^1(\theta_\varphi) \sigma_\varphi \quad (19)$$

$$\dot{\sigma}_\varphi = \kappa_\varphi^2(\theta_\varphi) + u_A, \quad (20)$$

where u_A is the torque applied at the stance ankle, d_φ is the last row of D_φ , and σ_φ is the angular momentum about the stance ankle during the fully-actuated phase [31]. Equations (19) and (20) are written as $\dot{z}_\varphi = f_{\mathcal{Z}_\varphi}(z_\varphi, u_A)$. The ankle torque u_A can be used either to shape the potential energy or to affect the convergence rate of the solution of the hybrid zero dynamics.

The transition map from the fully-actuated phase to the underactuated phase on the zero dynamics becomes

$$\theta_v^+ = \theta_v \circ \begin{bmatrix} q_\varphi^- \\ \pi \end{bmatrix} \quad (21)$$

$$\sigma_v^+ = \delta_\varphi^v \sigma_\varphi^-, \quad (22)$$

where δ_φ^v is a constant that can be calculated using [21].

C. Hybrid zero dynamics

Let \mathcal{Z}_φ be the zero dynamics manifold of the fully-actuated phase and $\dot{z}_\varphi = f_{\mathcal{Z}_\varphi}(z_\varphi, u_A)$ be the associated zero dynamics driven by u_A . Let Δ_φ^v be the transition map from the fully-actuated phase to the underactuated phase. Let \mathcal{Z}_v be the zero dynamics manifold of the underactuated phase and $\dot{z}_v = f_v(z_v)$ be the associated zero dynamics. Let Δ_v^φ be the transition map from the underactuated phase to the fully-actuated phase. If $\forall z_\varphi \in \mathcal{S}_\varphi^v \cap \mathcal{Z}_\varphi$, $\Delta_\varphi^v(z_\varphi) \in \mathcal{Z}_v$ and $\forall z_v \in \mathcal{S}_v^\varphi \cap \mathcal{Z}_v$, $\Delta_v^\varphi(z_v) \in \mathcal{Z}_\varphi$, then

$$\begin{cases} \dot{z}_\varphi = f_{\mathcal{Z}_\varphi}(z_\varphi, u_A), & z_\varphi^- \notin \mathcal{S}_\varphi^v \cap \mathcal{Z}_\varphi, u_A \in \mathbf{R} \\ z_\varphi^+ = \Delta_\varphi^v(z_\varphi), & z_\varphi^- \in \mathcal{S}_\varphi^v \cap \mathcal{Z}_\varphi \\ \dot{z}_v = f_v(z_v), & z_v^- \notin \mathcal{S}_v^\varphi \cap \mathcal{Z}_v \\ z_v^+ = \Delta_v^\varphi(z_v), & z_v^- \in \mathcal{S}_v^\varphi \cap \mathcal{Z}_v \end{cases} \quad (23)$$

is an invariant hybrid subsystem of the full-order hybrid model. The system (23) is called the *hybrid zero dynamics* and \mathcal{Z}_φ and \mathcal{Z}_v are hybrid zero dynamics manifolds.

Remark 2: By definition, \mathcal{Z}_φ and \mathcal{Z}_v are hybrid zero dynamics manifolds if, and only if, $\forall z_\varphi^- \in \mathcal{S}_\varphi^v \cap \mathcal{Z}_\varphi$,

$$h_v \circ \Delta_\varphi^v(z_\varphi^-) = 0, \quad (24)$$

$$L_{f_v} h_v \circ \Delta_\varphi^v(z_\varphi^-) = 0, \quad (25)$$

and $\forall z_v^- \in \mathcal{S}_v^\varphi \cap \mathcal{Z}_v$ and $u_A = 0$,

$$h_\varphi \circ \Delta_v^\varphi(z_v^-) = 0, \quad (26)$$

$$L_{f_\varphi} h_\varphi \circ \Delta_v^\varphi(z_v^-) = 0. \quad (27)$$

How to achieve these conditions is developed in Section V. \square

IV. ANKLE CONTROL AND STABILITY ANALYSIS

Due to the ankle torque that appears in the zero dynamics for the fully-actuated phase in (20), the robot's center of mass can move backward as well as forward during a step. In other words, the angular momentum about the stance ankle can be zero before entering the underactuated phase. We assume here, however, that the angular momentum is never zero during a step; see GH7 in Appendix I. One can think of this hypothesis as a difference between walking and dancing. Furthermore, during the underactuated phase, the angular momentum of the robot is never zero if the robot completes a step [21].

The ankle torque provides additional design freedom in the fully-actuated phase, which can be used for various purposes. In this paper, two possible usages of the ankle torque are suggested: changing the walking speed of the robot through potential-energy shaping; affecting the convergence rate to the periodic orbit. The stability of the robot on the hybrid zero dynamics is analyzed with a Poincaré map for the overall system, which can be obtained by composing the Poincaré map for each phase.

A. Analysis on the hybrid zero dynamics for the underactuated phase

For the underactuated phase, the zero dynamics is equivalent to the robot with unactuated point feet, [21]. If the robot completes a step, the angular momentum during the underactuated phase is never zero. Therefore, $\zeta_v = \frac{\sigma_v^2}{2}$ is a valid coordinate transformation, where σ_v is the angular momentum. Let $z_v^- = (\theta_v^-, \sigma_v^-) \in \mathcal{S}_v^\varphi \cap \mathcal{Z}_v$ and let θ_v^+ be defined as in (21). If $(\delta_v^\varphi)^2 \zeta_v^- - V_{\mathcal{Z}_v}^{max} > 0$, then following the procedure in [21] with (12) and (13) gives

$$\frac{1}{2}(\sigma_v^-)^2 - \frac{1}{2}(\sigma_v^+)^2 = \zeta_v^- - \zeta_v^+ = -V_{\mathcal{Z}_v}(\theta_v^-), \quad (28)$$

where

$$V_{\mathcal{Z}_v}(\theta_v) = - \int_{\theta_v^+}^{\theta_v} \frac{\kappa_v^2(\xi)}{\kappa_v^1(\xi)} d\xi, \quad (29)$$

$$V_{\mathcal{Z}_v}^{max} = \max_{\theta_v^+ \leq \theta_v \leq \theta_v^-} V_{\mathcal{Z}_v}(\theta_v). \quad (30)$$

The Poincaré map for the underactuated phase $\rho_v : \mathcal{S}_v^\varphi \cap \mathcal{Z}_v \rightarrow \mathcal{S}_v^\varphi \cap \mathcal{Z}_v$ on the hybrid zero dynamics is defined with (22) as

$$\rho_v(\zeta_v^-) = (\delta_v^\varphi)^2 \zeta_v^- - V_{\mathcal{Z}_v}(\theta_v^-). \quad (31)$$

B. Analysis on the hybrid zero dynamics for the fully-actuated phase with ankle torque used to change walking speed

An ankle torque control strategy that is useful for modifying the walking speed is proposed. The Poincaré map for the fully-actuated phase is then calculated, and the Poincaré map for the overall reduced system is determined for stability analysis of the robot on the hybrid zero dynamics.

Since the angular momentum of the robot during the fully-actuated phase, σ_φ , is not zero during the fully-actuated phase, $\zeta_\varphi = \frac{\sigma_\varphi^2}{2}$ is a valid coordinate transformation. For the purpose

of potential-energy shaping, the ankle torque during the fully-actuated phase, u_Δ , is assumed to be a function of θ_φ only. Then, (19) and (20) become

$$d\zeta_\varphi = \sigma_\varphi d\sigma_\varphi = \frac{\kappa_\varphi^2(\theta_\varphi)}{\kappa_\varphi^1(\theta_\varphi)} + \frac{u_\Delta(\theta_\varphi)}{\kappa_\varphi^1(\theta_\varphi)} d\theta_\varphi. \quad (32)$$

Let $z_\varphi^- = (\theta_\varphi^-, \sigma_\varphi^-) \in \mathcal{S}_\varphi^v \cap \mathcal{Z}_\varphi$ and θ_φ^+ be defined as in (14). For $\theta_\varphi^+ \leq \theta_\varphi \leq \theta_\varphi^-$, define

$$V_{\mathcal{Z}_\varphi}^{u_\Delta}(\theta_\varphi) = - \int_{\theta_\varphi^+}^{\theta_\varphi} \frac{\kappa_\varphi^2(\xi)}{\kappa_\varphi^1(\xi)} + \frac{u_\Delta(\xi)}{\kappa_\varphi^1(\xi)} d\xi, \quad (33)$$

$$V_{\mathcal{Z}_\varphi}^{u_\Delta, max} = \max_{\theta_\varphi^+ \leq \theta_\varphi \leq \theta_\varphi^-} V_{\mathcal{Z}_\varphi}^{u_\Delta}(\theta_\varphi). \quad (34)$$

If $(\delta_\varphi^v)^2 \zeta_\varphi^- - V_{\mathcal{Z}_\varphi}^{u_\Delta, max} > 0$, then (32) can be integrated, which results in

$$\frac{1}{2}(\sigma_\varphi^-)^2 - \frac{1}{2}(\sigma_\varphi^+)^2 = \zeta_\varphi^- - \zeta_\varphi^+ = -V_{\mathcal{Z}_\varphi}^{u_\Delta}(\theta_\varphi^-). \quad (35)$$

With (15), the Poincaré map for the fully-actuated phase on the hybrid zero dynamics, $\rho_\varphi : \mathcal{S}_\varphi^v \cap \mathcal{Z}_v \rightarrow \mathcal{S}_\varphi^v \cap \mathcal{Z}_v$, is defined as

$$\rho_\varphi(\zeta_v^-) = (\delta_v^\varphi)^2 \zeta_v^- - V_{\mathcal{Z}_\varphi}^{u_\Delta}(\theta_\varphi^-). \quad (36)$$

Hence, the Poincaré map for the overall reduced system in (θ_v, ζ_v) coordinates, $\rho(\zeta_v^-) : \mathcal{S}_v^\varphi \cap \mathcal{Z}_v \rightarrow \mathcal{S}_v^\varphi \cap \mathcal{Z}_v$, is defined as composition of (31) and (36) as follows.

$$\begin{aligned} \rho(\zeta_v^-) &= \rho_v \circ \rho_\varphi(\zeta_v^-) \\ &= (\delta_\varphi^v)^2 (\delta_v^\varphi)^2 \zeta_v^- - (\delta_\varphi^v)^2 V_{\mathcal{Z}_\varphi}^{u_\Delta}(\theta_\varphi^-) - V_{\mathcal{Z}_v}(\theta_v^-) \end{aligned} \quad (37)$$

with domain of definition

$$\begin{aligned} \mathcal{D} &= \{ \zeta_v^- > 0 \mid (\delta_v^\varphi)^2 \zeta_v^- - V_{\mathcal{Z}_\varphi}^{u_\Delta, max} > 0, \\ &(\delta_\varphi^v)^2 (\delta_v^\varphi)^2 \zeta_v^- - (\delta_\varphi^v)^2 V_{\mathcal{Z}_\varphi}^{u_\Delta}(\theta_\varphi^-) - V_{\mathcal{Z}_v}^{max}(\theta_v^-) > 0 \}. \end{aligned} \quad (38)$$

Theorem 1: Under the hypotheses RH1–RH5, GH1–GH7, and IH1–IH7 in Appendix I, HHF1–HHF5, and HHU1–HHU5,

$$\zeta_v^* = - \frac{(\delta_\varphi^v)^2 V_{\mathcal{Z}_\varphi}^{u_\Delta}(\theta_\varphi^-) + V_{\mathcal{Z}_v}(\theta_v^-)}{1 - (\delta_\varphi^v)^2 (\delta_v^\varphi)^2} \quad (39)$$

is an exponentially stable fixed point of (37) if, and only if,

$$0 < (\delta_\varphi^v)^2 (\delta_v^\varphi)^2 < 1, \quad (40)$$

$$\frac{(\delta_\varphi^v)^2 (\delta_v^\varphi)^2 V_{\mathcal{Z}_v} + (\delta_\varphi^v)^2 V_{\mathcal{Z}_\varphi}^{u_\Delta}}{1 - (\delta_\varphi^v)^2 (\delta_v^\varphi)^2} + V_{\mathcal{Z}_v}^{max} < 0, \quad (41)$$

$$\frac{(\delta_\varphi^v)^2 (\delta_v^\varphi)^2 V_{\mathcal{Z}_\varphi}^{u_\Delta} + (\delta_\varphi^v)^2 V_{\mathcal{Z}_v}}{1 - (\delta_\varphi^v)^2 (\delta_v^\varphi)^2} + V_{\mathcal{Z}_\varphi}^{u_\Delta, max} < 0. \quad (42)$$

Proof: \mathcal{D} is non-empty if, and only if, $(\delta_\varphi^v)^2 (\delta_v^\varphi)^2 > 0$. If there exists $\zeta_v^* \in \mathcal{D}$ satisfying $\rho(\zeta_v^*) = (\delta_\varphi^v)^2 (\delta_v^\varphi)^2 \zeta_v^* - (\delta_\varphi^v)^2 V_{\mathcal{Z}_\varphi}^{u_\Delta}(\theta_\varphi^-) - V_{\mathcal{Z}_v}(\theta_v^-)$, then ζ_v^* is an exponentially stable fixed point if, and only if, $0 < (\delta_\varphi^v)^2 (\delta_v^\varphi)^2 < 1$, and in this case, (39) is the value of ζ_v^* . Finally, (41) and (42) are the necessary and sufficient conditions for (39) to be in \mathcal{D} . ■

Remark 3: The stability of the reduced model is not affected by the choice of $u_\Delta(\theta_\varphi)$ since δ_φ^v does not depend on u_Δ . However, the fixed point ζ_v^* is affected by u_Δ . □

C. Analysis on the hybrid zero dynamics for fully-actuated phase with ankle torque used to affect convergence rate

It is now shown how the ankle torque can be used to affect the stability of the robot on the hybrid zero dynamics; In particular the torque is used to affect convergence rate. For the analysis, the Poincaré map for the fully-actuated phase is calculated and then composed with the Poincaré map of the underactuated phase to provide the Poincaré map of the overall reduced system.

Due to the assumption GH7, which assumes non-zero angular momentum during the fully-actuated phase, $\zeta_\varphi = \frac{\sigma_\varphi^2}{2}$ is a valid coordinate transformation. Define the ankle torque u_A to be

$$u_A = -\kappa_\varphi^2(\theta_\varphi) + \kappa_\varphi^1(\theta_\varphi) \left(a(\zeta_\varphi - \zeta_\varphi^*(\theta_\varphi)) + \frac{d\zeta_\varphi^*(\theta_\varphi)}{d\theta_\varphi} \right), \quad (43)$$

where a is a negative constant, $\zeta_\varphi^*(\theta_\varphi)$ is a function of θ_φ only, which describes the desired path of ζ_φ during the fully-actuated phase, and $\kappa_\varphi^1(\theta_\varphi)$ and $\kappa_\varphi^2(\theta_\varphi)$ are from (19) and (20), respectively. Then the zero dynamics becomes

$$\dot{\theta}_\varphi = \kappa_\varphi^1(\theta_\varphi)\sigma_\varphi \quad (44)$$

$$\dot{\zeta}_\varphi = \kappa_\varphi^1(\theta_\varphi) \left(a(\zeta_\varphi - \zeta_\varphi^*(\theta_\varphi)) + \frac{d\zeta_\varphi^*(\theta_\varphi)}{d\theta_\varphi} \right). \quad (45)$$

In $(\theta_\varphi, \zeta_\varphi)$ coordinates, combining (44) and (45) yields

$$\frac{d\zeta_\varphi}{d\theta_\varphi} = a(\zeta_\varphi - \zeta_\varphi^*(\theta_\varphi)) + \frac{d\zeta_\varphi^*(\theta_\varphi)}{d\theta_\varphi}. \quad (46)$$

Define $\eta = \zeta_\varphi - \zeta_\varphi^*(\theta_\varphi)$. Then, with (46), differentiating η gives

$$\frac{d\eta}{d\theta_\varphi} = \frac{d\zeta_\varphi}{d\theta_\varphi} - \frac{d\zeta_\varphi^*(\theta_\varphi)}{d\theta_\varphi} \quad (47)$$

$$= a(\zeta_\varphi - \zeta_\varphi^*(\theta_\varphi)) = a\eta, \quad (48)$$

which can be solved for $\theta_\varphi^+ \leq \theta_\varphi \leq \theta_\varphi^-$ to give

$$\eta(\theta_\varphi) = e^{a(\theta_\varphi - \theta_\varphi^+)} \eta(\theta_\varphi^+). \quad (49)$$

Therefore,

$$\zeta_\varphi = \zeta_\varphi^*(\theta_\varphi) + e^{a(\theta_\varphi - \theta_\varphi^+)} (\zeta_\varphi^+ - \zeta_\varphi^*(\theta_\varphi^+)). \quad (50)$$

Since $\theta_\varphi = \theta_\varphi^-$ at the transition from the fully-actuated phase to the underactuated phase,

$$\zeta_\varphi^- = \zeta_\varphi^*(\theta_\varphi^-) + e^{a(\theta_\varphi^- - \theta_\varphi^+)} (\zeta_\varphi^+ - \zeta_\varphi^*(\theta_\varphi^+)). \quad (51)$$

The Poincaré map for the fully-actuated phase, $\rho_\varphi : \mathcal{S}_\varphi^\varphi \cap \mathcal{Z}_v \rightarrow \mathcal{S}_\varphi^v \cap \mathcal{Z}_v$, is therefore given as

$$\rho_\varphi(\zeta_\varphi^-) = (\delta_v^\varphi)^2 e^{a(\theta_\varphi^- - \theta_\varphi^+)} \zeta_\varphi^- + \zeta_\varphi^*(\theta_\varphi^-) - e^{a(\theta_\varphi^- - \theta_\varphi^+)} \zeta_\varphi^*(\theta_\varphi^+). \quad (52)$$

Combining (31) and (52) gives the Poincaré map for the overall reduced system; in (θ_v, ζ_v) coordinates, $\rho(\zeta_v^-) = \rho_v \circ \rho_\varphi(\zeta_v^-) : \mathcal{S}_v^\varphi \cap \mathcal{Z}_v \rightarrow \mathcal{S}_v^\varphi \cap \mathcal{Z}_v$, as follows:

$$\begin{aligned} \rho(\zeta_v^-) &= (\delta_v^\varphi)^2 (\delta_v^v)^2 e^{a(\theta_\varphi^- - \theta_\varphi^+)} \zeta_v^- + (\delta_v^v)^2 (\zeta_\varphi^*(\theta_\varphi^-) \\ &\quad - e^{a(\theta_\varphi^- - \theta_\varphi^+)} \zeta_\varphi^*(\theta_\varphi^+)) - V_{\mathcal{Z}_v}(\theta_v^-) \end{aligned}$$

with domain of definition

$$\mathcal{D} = \{\zeta_v^- \in \mathbb{R} \mid \zeta_v^- > 0\}. \quad (53)$$

Theorem 2: Assume the hypotheses RH1–RH5, GH1–GH7, and IH1–IH7 in Appendix I, HHF1–HHF5, and HHU1–HHU5 are satisfied. Let ζ^* be a differentiable function of θ_φ , satisfying the following conditions,

$$\zeta_\varphi^*(\theta_\varphi) > 0, \quad \forall \theta_\varphi \in [\theta_\varphi^+, \theta_\varphi^-] \quad (54)$$

$$(\delta_v^\varphi)^2 (\delta_v^v)^2 \zeta_\varphi^*(\theta_\varphi^-) - \zeta_\varphi^*(\theta_\varphi^+) = (\delta_v^v)^2 V_{\mathcal{Z}_v}(\theta_v^-). \quad (55)$$

Then,

$$\zeta_v^* = \frac{(\delta_v^\varphi)^2 \zeta_\varphi^*(\theta_\varphi^-) - (\delta_v^v)^2 e^{a(\theta_\varphi^- - \theta_\varphi^+)} \zeta_\varphi^*(\theta_\varphi^+) - V_{\mathcal{Z}_v}(\theta_v^-)}{1 - (\delta_v^\varphi)^2 (\delta_v^v)^2 e^{a(\theta_\varphi^- - \theta_\varphi^+)}} \quad (56)$$

is an exponentially stable fixed point of (53) if, and only if,

$$0 < (\delta_v^\varphi)^2 (\delta_v^v)^2 e^{a(\theta_\varphi^- - \theta_\varphi^+)} < 1, \quad a < 0 \quad (57)$$

$$(\delta_v^\varphi)^2 \zeta_\varphi^*(\theta_\varphi^-) - V_{\mathcal{Z}_v}^{max} > 0 \quad (58)$$

Proof: The domain of definition, \mathcal{D} , is non-empty if, and only if, (58) is satisfied. If there exists $\zeta_v^* \in \mathcal{D}$ satisfying $\zeta^* = \rho(\zeta^*)$, where ρ is the Poincaré map defined in (53), then, ζ^* is an exponentially fixed point if, and only if, (57) is satisfied, in which case the value of the fixed point is given as (56). ■

Remark 4: The convergence rate of the solution to the limit cycle can be altered by the ankle torque, u_A , through choice of a , as long as the constraint on the FRI point during the fully-actuated phase is satisfied. □

D. Stability of the robot in the full-order model

A very important result not proved in the paper is that asymptotically stable periodic orbits of the hybrid zero dynamics are *asymptotically stabilizable* in the full-order model. The proof is based on extending the main result of [20]. For an analogous result in running, see [29].

V. DESIGNING THE VIRTUAL CONSTRAINTS

To render the analytical results in the previous section useful for feedback design, a convenient finite parametrization of the virtual constraints and the angular momentum during the fully-actuated phase must be introduced as in [21, Sec. V]. This introduces free parameters into the hybrid zero dynamics, (23). A minimum cost criterion can then be posed and parameter optimization applied to the hybrid zero dynamics to design a provably stable, closed-loop system with satisfied design constraints, such as walking at a prescribed average speed, the forces on the support leg lying in the allowed friction cone, and the foot rotation indicator point within the hull of the foot during the fully-actuated phase and strictly in front of the foot in the underactuated phase.

A. Parametrization using Bézier polynomials

For the parametrization of the output function for each phase, Bézier polynomials are used. Let

$$b_\varphi^i(s_\varphi) := \sum_{k=0}^{M_\varphi} \alpha_k^i \frac{M_\varphi!}{k!(M_\varphi - k)!} s_\varphi^k (1 - s_\varphi)^{M_\varphi - k}, \quad (59)$$

$$b_v^i(s_v) := \sum_{k=0}^{M_v} \beta_k^i \frac{M_v!}{k!(M_v - k)!} s_v^k (1 - s_v)^{M_v - k}, \quad (60)$$

where $M_\varphi > 3$, $M_v > 3$, $s_\varphi(\theta_\varphi) = \frac{\theta_\varphi - \theta_\varphi^+}{\theta_\varphi^- - \theta_\varphi^+}$ and $s_v(\theta_v) = \frac{\theta_v - \theta_v^+}{\theta_v^- - \theta_v^+}$. Note that $s_\varphi = 0$, $s_\varphi = 1$, $s_v = 0$, and $s_v = 1$ represent the beginning and the end of the fully-actuated phase and the beginning and the end of the underactuated phase, respectively. Define the output function for each phase, satisfying the output hypotheses in Section III, to be

$$y_\varphi = h_\varphi(q_\varphi) = h_\varphi^t(q_\varphi) - h_\varphi^d \circ \theta_\varphi(q_\varphi) \quad (61)$$

$$y_v = h_v(q_v) = h_v^t(q_v) - h_v^d \circ \theta_v(q_v), \quad (62)$$

where h_φ^t is a vector with $N - 2$ elements specifying independent entities to be controlled during fully-actuated phase, h_v^t is a vector containing $N - 1$ independent values to be controlled during underactuated phase, $h_\varphi^d(\theta_\varphi)$ and $h_v^d(\theta_v)$ are the desired curves for the controlled elements to track during each phase. The desired curves, $h_\varphi^d(\theta_\varphi)$ and $h_v^d(\theta_v)$, are defined as follows.

$$h_\varphi^d(\theta_\varphi) = \begin{bmatrix} b_\varphi^1 \circ s_\varphi(\theta_\varphi) \\ \dots \\ b_\varphi^{N-2} \circ s_\varphi(\theta_\varphi) \end{bmatrix}, \quad (63)$$

$$h_v^d(\theta_v) = \begin{bmatrix} b_v^1 \circ s_v(\theta_v) \\ \dots \\ b_v^{N-1} \circ s_v(\theta_v) \end{bmatrix}. \quad (64)$$

Note that due to the properties of the Bézier polynomials, the desired output function at the beginning of each phase is

$$h_\varphi^d(s_\varphi)|_{s_\varphi=0} = \alpha_0 \quad (65)$$

$$\left. \frac{\partial h_\varphi^d(s_\varphi)}{\partial s_\varphi} \right|_{s_\varphi=0} = M_\varphi(\alpha_1 - \alpha_0) \quad (66)$$

$$h_v^d(s_v)|_{s_v=0} = \beta_0 \quad (67)$$

$$\left. \frac{\partial h_v^d(s_v)}{\partial s_v} \right|_{s_v=0} = M_v(\beta_1 - \beta_0), \quad (68)$$

and, similarly, at the end of each phase is

$$h_\varphi^d(s_\varphi)|_{s_\varphi=1} = \alpha_{M_\varphi} \quad (69)$$

$$\left. \frac{\partial h_\varphi^d(s_\varphi)}{\partial s_\varphi} \right|_{s_\varphi=1} = M_\varphi(\beta_{M_\varphi} - \beta_{M_\varphi-1}) \quad (70)$$

$$h_v^d(s_v)|_{s_v=1} = \beta_{M_v} \quad (71)$$

$$\left. \frac{\partial h_v^d(s_v)}{\partial s_v} \right|_{s_v=1} = M_v(\beta_{M_v} - \beta_{M_v-1}), \quad (72)$$

where

$$\alpha_i = \begin{bmatrix} \alpha_i^1 \\ \vdots \\ \alpha_i^{N-2} \end{bmatrix}, \quad i = 0, \dots, M_\varphi \quad (73)$$

$$\beta_j = \begin{bmatrix} \beta_j^1 \\ \vdots \\ \beta_j^{N-1} \end{bmatrix}, \quad j = 0, \dots, M_v \quad (74)$$

When the ankle torque is used to affect the stability as explained in Section IV-C, the desired path of the angular momentum also needs to be designed. Since the angular momentum during the fully-actuated phase is never zero, $\zeta^* = \frac{(\sigma^*)^2}{2}$ is parameterized instead of the desired angular momentum, σ^* , which is given by

$$\zeta^* \circ s_\varphi(\theta_\varphi) := \sum_{k=0}^m \gamma_k \frac{m!}{k!(m-k)!} s_\varphi^k (1 - s_\varphi)^{m-k}, \quad (75)$$

where $m > 1$. By the properties of Bézier polynomials,

$$\zeta^*(s_\varphi)|_{s_\varphi=0} = \gamma_0 \quad (76)$$

$$\zeta^*(s_\varphi)|_{s_\varphi=1} = \gamma_m. \quad (77)$$

B. Achieving invariance of the hybrid zero dynamics

To achieve the invariance, the output function for each phase needs to be designed such that the invariance conditions (24), (25), (26), and (27) are satisfied. Since y_φ and y_v satisfy HHF3 and HHU3, respectively, $[h_\varphi(q_\varphi); \theta_\varphi(q_\varphi)]$ and $[h_v(q_v); \theta_v(q_v)]$ are invertible, which holds if, and only if,

$$H_\varphi(q_\varphi) := \begin{bmatrix} h_\varphi^t(q_\varphi) \\ \theta_\varphi(q_\varphi) \end{bmatrix} \quad (78)$$

and

$$H_v(q_v) := \begin{bmatrix} h_v^t(q_v) \\ \theta_v(q_v) \end{bmatrix} \quad (79)$$

are invertible. By definition, on the zero dynamics manifold for each phase, the output function satisfies the following conditions.

$$y_\varphi = h_\varphi(q_\varphi) = h_\varphi^t(q_\varphi) - h_\varphi^d \circ \theta_\varphi(q_\varphi) = 0, \quad (80)$$

$$y_v = h_v(q_v) = h_v^t(q_v) - h_v^d \circ \theta_v(q_v) = 0. \quad (81)$$

Since $H_\varphi(q_\varphi)$ and $H_v(q_v)$ are invertible, the condition for the position states after the transition to remain in the zero dynamics manifold for the underactuated phase is derived as

$$\begin{bmatrix} \beta_0 \\ \theta_v(q_v^+) \end{bmatrix} = H_v \circ \left[H_\varphi^{-1} \circ \begin{bmatrix} \alpha_{M_\varphi} \\ \theta_\varphi(q_\varphi^-) \end{bmatrix} \right]. \quad (82)$$

Similarly, the condition for the position states to be in the zero dynamics manifold for the fully-actuated phase after the transition from the underactuated phase to the fully-actuated can be obtained to be

$$\begin{bmatrix} \alpha_0 \\ \theta_\varphi(q_\varphi^+) \end{bmatrix} = H_\varphi \circ \left(\begin{bmatrix} R & 0 \end{bmatrix} \left(H_v^{-1} \circ \begin{bmatrix} \beta_{M_v} \\ \theta_v(q_v^-) \end{bmatrix} \right) \right), \quad (83)$$

where R is the relabeling matrix.

Since $\dot{y}_\varphi = 0$ and $\dot{y}_v = 0$ on the zero dynamics manifold for each phase,

$$\dot{y}_\varphi = \frac{\partial h_\varphi^t(q_\varphi)}{\partial q_\varphi} \dot{q}_\varphi - \frac{\partial h_\varphi^d}{\partial s_\varphi} \frac{\partial s_\varphi}{\partial \theta_\varphi} \dot{\theta}_\varphi = 0, \quad (84)$$

$$\dot{y}_v = \frac{\partial h_v^t(q_v)}{\partial q_v} \dot{q}_v - \frac{\partial h_v^d}{\partial s_v} \frac{\partial s_v}{\partial \theta_v} \dot{\theta}_v = 0. \quad (85)$$

Since $H_\varphi(q_\varphi)$ and $H_v(q_v)$ are invertible, the condition for the velocity states after the transition from the fully-actuated phase to the underactuated phase to be in the zero dynamics manifold for the underactuated phase can be obtained from the transition map (7) as

$$\beta_1 = \frac{\theta_\varphi^- - \theta_\varphi^+}{M_\varphi} \frac{\partial h_\varphi^t}{\partial q_\varphi} \Sigma \frac{\kappa_\varphi^1(\theta_\varphi^-)}{\kappa_\varphi^1(\theta_\varphi^+) \delta_\varphi^v} + \beta_0, \quad (86)$$

where

$$\Sigma = \left(\left[\begin{array}{c} \frac{\partial H_\varphi}{\partial q_\varphi}^{-1} \left[\begin{array}{c} \frac{M_\varphi(\alpha_{M_\varphi} - \alpha_{M_\varphi-1})}{\theta_\varphi^- - \theta_\varphi^+} \\ 1 \end{array} \right] \\ 0 \end{array} \right] \right). \quad (87)$$

Similarly, the condition for the velocity states to be in the zero dynamics manifold for the fully-actuated after the transition can be obtained as

$$\alpha_1 = \frac{\theta_\varphi^- - \theta_\varphi^+}{M_\varphi} \frac{\partial h_\varphi^t}{\partial q_\varphi} \Delta_{\dot{q}_\varphi, v}^\varphi(q_v^-) \frac{\partial H_v}{\partial q_v}^{-1} \Xi \frac{\kappa_v^1(\theta_v^-)}{\kappa_v^1(\theta_v^+) \delta_v^v} + \alpha_0, \quad (88)$$

where

$$\Xi = \left[\begin{array}{c} \frac{M_v(\beta_{M_v} - \beta_{M_v-1})}{\theta_v^- - \theta_v^+} \\ 1 \end{array} \right]. \quad (89)$$

When the ankle torque is controlled to affect the stability, the desired path of the angular momentum during the fully-actuated phase, $\zeta_\varphi^*(s_\varphi)$, needs to satisfy (54), which is essentially equivalent to non-zero angular momentum hypothesis GH7, and (55) for periodicity. Since $\zeta_\varphi^*(\theta_\varphi^+) = \gamma_0$ and $\zeta_\varphi^*(\theta_\varphi^-) = \gamma_m$, the condition for γ_0 is given by

$$\gamma_0 = (\delta_\varphi^v)^2 (\delta_v^v)^2 \gamma_m - (\delta_v^v)^2 V_{Z_v}(\theta_v^-), \quad (90)$$

from (55).

C. Specifying the remaining free parameters

There are free coefficients in the Bézier polynomials after meeting the invariance conditions and they can be used to satisfy constraints for stability, friction to realize non-slipping, anthropomorphic gait, average walking speed, etc. This section explains the various constraints.

Equality constraint:

IEC1) Average walking speed is constant. The walking speed of the robot, which is defined as step length divided by time duration of a step, is given by

$$v = \frac{L_s}{T_s}, \quad (91)$$

where L_s is the step length and T_s is the time elapsed for the step.

Inequality constraints:

IEC1) The stability condition (57) is satisfied;

IEC2) The non-slipping assumption is satisfied. In each phase, the foot will not slip if the ratio of the tangential reaction force and the normal reaction force from the ground are within the friction cone, which can be formulated as

$$\left| \frac{F_T}{F_N} \right| \leq \mu, \quad (92)$$

where μ is the Coulomb friction coefficient of the surface and F_T is the tangential force, and F_N is the normal reaction force;

IEC3) The normal reaction force from the ground is positive.

This is due to the fact that the ground reaction force is unilateral. In other words, the ground cannot pull the robot down;

IEC4) The height of the swing foot is positive during step;

IEC5) The FRI point is within the stance footprint (i.e. the convex hull of the foot);

IEC6) The stance foot leaves the ground after the double support;

IEC7) The angles of the knees and ankles are limited to produce anthropomorphic gait;

IEC8) The torque applied at each joint is limited to a physically realizable value.

The desired output functions and the desired angular momentum during a step need to be determined, subject to the invariance condition and the constraints being satisfied. This can be formulated as an numerical optimization problem. The cost function used here is defined as

$$J = \frac{1}{L_s} \int_{T_I^+}^{T_I^-} \sum_{k=1}^N |\dot{q}_k u_k| dt, \quad (93)$$

where L_s is the step length, T_I^+ and T_I^- are the time of beginning and end of the step, respectively.

VI. SIMULATION

For an illustration, a planar bipedal robot with 7-rigid links is used. See Figure 3 for the detailed coordinate conventions. The degrees of the polynomials used in the desired output functions and desired angular momentum for both phases are set to be $M_\varphi = 6$, $M_v = 6$, and $m = 5$. The parameters used for the simulation are given in Table I. The parameters are defined as shown in Figure 6.

Figure 7 and Figure 8 show the position and velocity states of the robot. During the underactuated phase, the angle of the stance foot decreases, which implies that the robot rolls over the stance toe.

Let $(0, 0)^\top$ be the Cartesian coordinate of the stance toe and let $(p_h^h, 0)^\top$ be the location of the stance heel during the fully-actuated phase, see Figure 3. In order for the stance foot not to rotate, the location of the FRI point, $(p_{FRI}^h, 0)^\top$ needs to satisfy

$$p_h^h < p_{FRI}^h < 0. \quad (94)$$

The location of the FRI point is shown in Figure 9, which satisfies (94), indicating the stance foot remains on the ground during the fully-actuated phase.

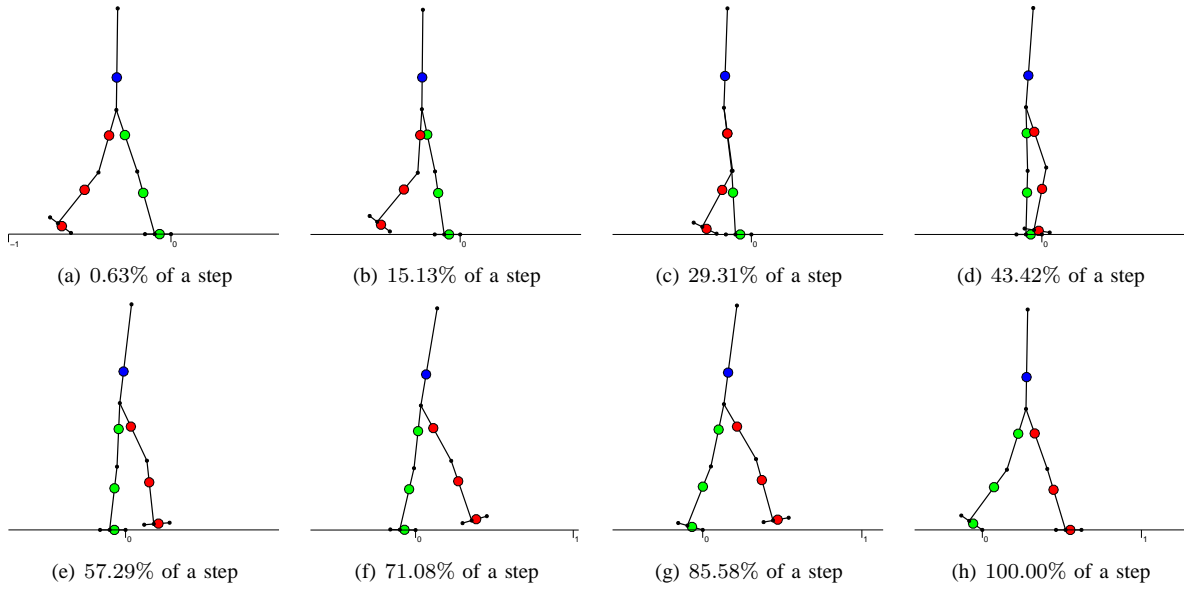


Fig. 11. Stick diagram of the robot during one step

Model Parameter	Units	Link	Label	Value
Mass	kg	Torso	M_{Torso}	36.044
		Femur	M_{Femur}	9.149
		Tibia	M_{Tibia}	3.000
		Foot	M_{Foot}	0.200
Length	m	Torso	L_{Torso}	0.625
		Femur	L_{Femur}	0.400
		Tibia	L_{Tibia}	0.400
		Toe	L_{Toe}	0.100
		Heel	L_{Heel}	0.060
Inertia	$m^2 kg$	Torso	I_{Torso}	5.527
		Femur	I_{Femur}	0.331
		Tibia	I_{Tibia}	0.149
		Foot	I_{Foot}	0.100
Mass center	m	Torso	l_{Torso}	0.200
		Femur	l_{Femur}	0.163
		Tibia	l_{Tibia}	0.137
		Foot	l_{Foot}	0.030

 TABLE I
 PARAMETERS FOR SIMULATION.

The applied torques are shown in Figure 10. Note that the torques have a discontinuity at the transition from the fully-actuated phase to the underactuated phase, which is allowed in this study. Figure 11 shows the gait of the robot during a step.

VII. SPECIAL CASE

The previous analysis can be specialized to a gait without foot rotation, in other words, to a gait with only flat-footed walking. This allows the differences with the ZMP criterion to be highlighted in the next section.

The stability conditions can be derived by specializing the calculations in Section IV to this case, the Poincaré map of the hybrid zero dynamics is ⁶

$$\rho(\zeta_v^-) = (\delta_v^\varphi)^2 \zeta_v^- - V_{Z_\varphi}^{uA}(\theta_\varphi^-), \quad (95)$$

⁶Conceptually, we are considering an instantaneous underactuated phase so that $V_{Z_v}(\theta_v^-) = 0$ and $\delta_v^\varphi = 1$

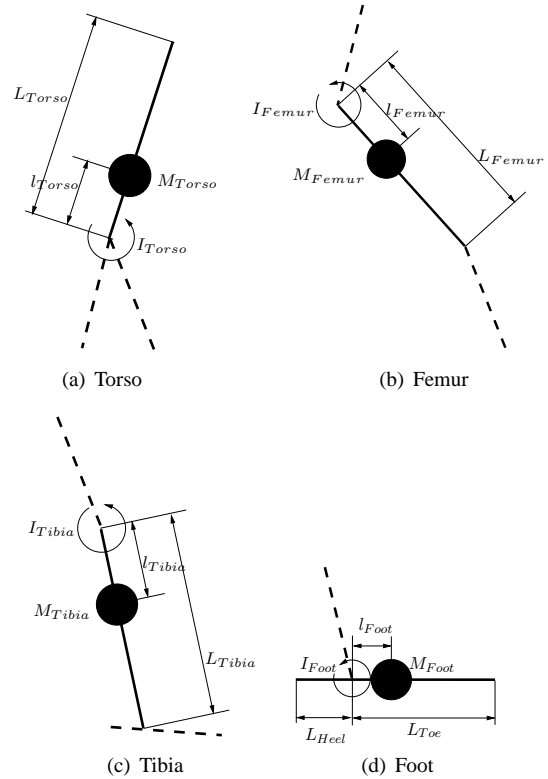


Fig. 6. Parameter definition for each link.

where $V_{Z_\varphi}^{uA}$, the potential energy (see [23]), is given in (33). The stability theorem becomes

Corollary 1: Under the hypotheses RH1–RH5, GH1–GH7, and IH1–IH7 in Appendix I, HHF1–HHF5,

$$\zeta_\varphi^* = -\frac{V_{Z_\varphi}^{uA}(\theta_\varphi^-)}{1 - (\delta_v^\varphi)^2} \quad (96)$$

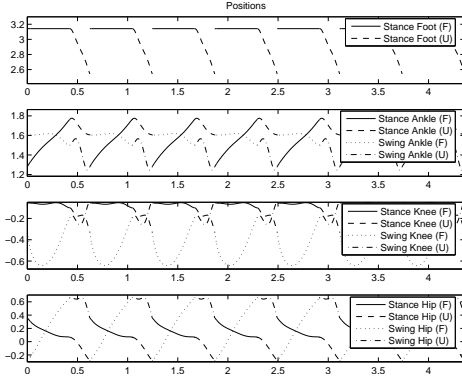


Fig. 7. Position states of the robot on HZD. The robot is walking at 1 m/s. F and U represent the fully-actuated and underactuated phases, respectively.

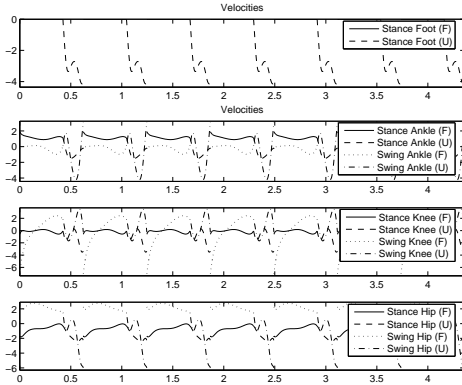


Fig. 8. Velocity states of the robot on HZD. The robot is walking at 1 m/s. F and U represent the fully-actuated and underactuated phases, respectively.

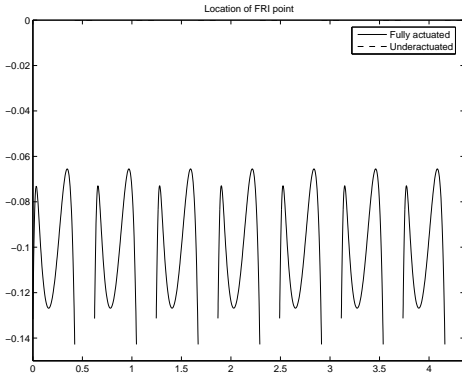


Fig. 9. Location of the FRI point. The robot is walking at 1 m/s. The discontinuity of the FRI point is due to the discontinuity in the torque at each transition.

is an exponentially stable fixed point of (95) if, and only if,

$$0 < (\delta_v^\varphi)^2 < 1, \quad (97)$$

$$\frac{(\delta_v^\varphi)^2 V_{Z_\varphi}^{u_A}(\theta_\varphi^-)}{1 - (\delta_v^\varphi)^2} + V_{Z_\varphi}^{u_A, max} < 0. \quad (98)$$

These conditions are the same as in [21, Th. 3] for point-feet, with the exception that the potential energy term $V_{Z_\varphi}^{u_A}$ can be shaped by choice of the ankle torque, u_A ; see second term in (33).

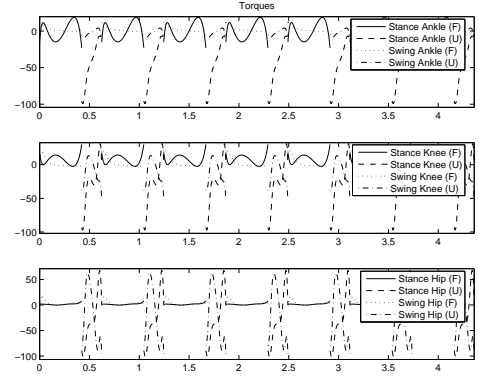


Fig. 10. Torques of the robot. F and U represent the fully-actuated and underactuated phases, respectively.

VIII. ZMP AND STABILITY OF AN ORBIT

The ZMP has been widely used as an indication of balance of a bipedal robot [5], [14], [4], [6], [32], [33], [34]. The ZMP being within the stance footprint is a sufficient and necessary condition for the stance foot not to rotate, but it does not mean the resulting walking motion is stable in the sense of a periodic orbit. In this section, only the special case of flat-footed walking is considered in order to illustrate that the ZMP principle alone is not sufficient for the stability of the robot.

	δ_v^φ	$V_{Z_\varphi}^{u_A}(\theta_\varphi^-)$ (kgm^2/s) ²	$V_{Z_\varphi}^{u_A, max}$ (kgm^2/s) ²	ζ_φ^* (kgm^2/s) ²
Value	1.266	505.213	1050.320	1678.309

TABLE II

QUANTITIES OF THE POINCARÉ RETURN MAP OF THE HYBRID ZERO DYNAMICS FOR AN UNSTABLE GAIT

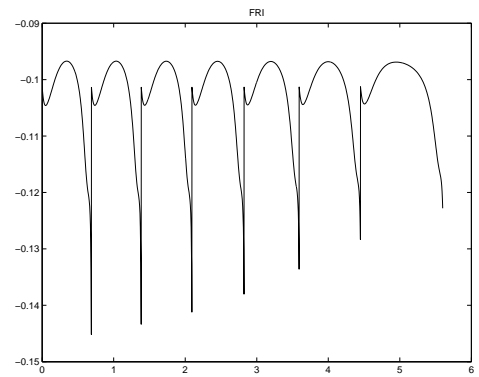


Fig. 12. Location of FRI point of an unstable gait. The FRI point remains within the stance footprint, $-0.16 < p_{FRI}^h < 0$.

Consider a planar bipedal robot whose gait consists only of the fully-actuated phase followed by an instantaneous double-support phase. The method of Section V was used to design a periodic orbit of the robot such that: (a) the FRI point is within the stance footprint during the fully-actuated phase in order for the stance foot to remain flat on the ground; (b) $(\delta_v^\varphi)^2$ in (95) is greater than one. See Table II. Note that if

the stance foot does not rotate, the FRI point is equivalent to the ZMP. The ankle torque is used for shaping the potential energy in this illustration.

Figure 12 shows the FRI point during the fully-actuated phase. Since the location of the FRI point satisfies (94), the stance foot does not rotate and the ZMP principle would “predict” stability. The gait, however, is not stable since the walking speed becomes slower when there is a small error in the velocity states at the initial conditions as shown in Figure 13. In this simulation, the velocity initial conditions are set to 99.5% of their value on the periodic orbit.

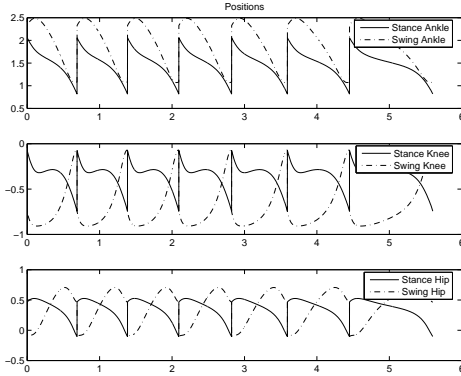


Fig. 13. Position states of robot with an unstable gait when the velocity states when the initial condition are 99.5% of their values on the periodic orbit.

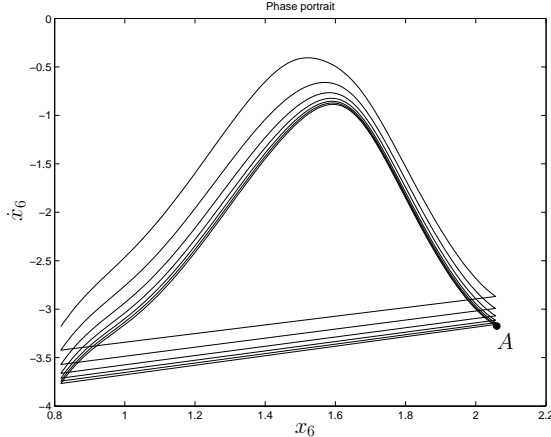


Fig. 14. Phase portrait of the absolute angle of the robot with an unstable gait. The point A represents the initial condition whose velocity states are 99.5% of their values on the periodic orbit.

Even with the unstable gait, the hybrid zero dynamics is invariant. Figure 14 shows the phase portrait of the absolute angle of the robot. The point A represents the initial condition. The gait of the robot diverges from the limit cycle, which implies that the periodic orbit is not stable.

Table II shows the Poincaré analysis of the unstable gait. Since $\delta_v^\varphi = 1.266$, the condition (97) is not satisfied, which causes instability.

IX. CONCLUSION

This paper has provided a solution to the key problem of walking with both fully-actuated and underactuated phases.

The studied robot was planar, bipedal, and fully actuated in the sense that it has non-trivial feet with revolute, actuated ankles and all other joints are independently actuated. The desired walking motion was assumed to consist of three successive phases: a fully-actuated phase where the stance foot is flat on the ground, an underactuated phase where the stance heel lifts from the ground and the stance foot rotates about the toe, and an instantaneous double-support phase where leg exchange takes place. The main contribution of the chapter was to extend the hybrid zero dynamics of [21] to a hybrid model with multiple continuous phases and varying degree of freedom and degrees of actuation. The developed method provides a provably asymptotically stabilizing controller that integrates the fully-actuated and underactuated phases of walking. Two possible usage of the ankle torque were suggested. The ankle torque was seen as a means either to directly adjust the potential energy of the hybrid zero dynamics or to affect the convergence rate of the solution to the limit cycle. The FRI point, or equivalently the ZMP, was used to ensure non-rotation of the stance foot, but not for the stability proof. The stability of the gait was shown via a Poincaré map on the hybrid zero dynamics. It was pointed out that the trajectories of the robot that keep the FRI point inside of the stance foot do not necessarily produce a stable gait.

APPENDIX I

HYPOTHESES FOR WALKING WITH FOOT ROTATION

The following hypotheses are used for walking with foot rotation. The hypotheses for the robot are:

- RH1) The robot consists of N rigid links with revolute joints;
- RH2) The robot is planar;
- RH3) The robot is bipedal with identical legs connected at hips;
- RH4) The joints between adjacent links are actuated;
- RH5) The coordinate of the robot consists of $N - 1$ relative angles, q_1, \dots, q_{N-1} , and one absolute angle, q_N .

The hypotheses for gait are:

- GH1) Walking consists of three successive phases, fully-actuated phase, underactuated phase, and double support phase;
- GH2) The stance foot remains on the ground during fully-actuated phase;
- GH3) The stance foot does not slip during fully-actuated phase;
- GH4) The stance toe acts as a pivot during underactuated phase;
- GH5) The stance ankle leaves the ground without interaction;
- GH6) There is no discontinuous change in positions and velocities at transition from fully-actuated phase to underactuated phase;
- GH7) The angular momentum about the stance ankle during the fully-actuated phase is not zero with presence of input.

The hypotheses for impact are:

- IH1) The swing foot has neither rebound nor slipping during impact;

- IH2) After impact, the stance toe leaves the ground without any interaction with the ground;
- IH3) The impact is instantaneous;
- IH4) The reaction forces due to the impact can be modeled as impulses;
- IH5) The impulsive forces result in discontinuous changes in the velocities while the position states remain continuous;
- IH6) The actuators at joints are not impulsive;
- IH7) The swing heel and the swing toe touch the ground at the same time.

The hypotheses for the closed-loop chain of double integrators, $\ddot{j} = \nu$, are:

- CH2) Existence of solutions on \mathbb{R}^{2N-2} and uniqueness;
- CH3) Solutions depending continuously on the initial conditions;
- CH4) The origin being globally asymptotically stable and the convergence being achieved in finite time;
- CH5) The settling time depending continuously on the initial condition.

APPENDIX II

FOOT ROTATION INDICATOR POINT DURING THE FULLY-ACTUATED PHASE

Note to the reviewer: Given the length of the paper, we plan to remove this section from the final paper and place it on the web. The calculations are straightforward. We will also include a citation to [35, Appendix G], where the result can also be found. The FRI point is defined in [26] as “the point on the foot/ground contact surface, within or outside the convex hull of the foot-support area, at which the resultant moment of the force/torque impressed on the foot is normal to the surface.” If the stance foot is motionless on the ground as assumed during the fully-actuated phase, then the Foot Rotation Indicator (FRI) point becomes equivalent to the Zero Moment Point (ZMP), which is within the stance footprint. Calculating the FRI point for the fully-actuated phase involves two phases. First, assume the stance foot is flat on the ground and calculate the FRI point. Second, validate the assumption by checking the location of the FRI point, which needs to be within the stance footprint.

Suppose the hypotheses RH1–RH2, RH5, and GH2–GH3 in Appendix I are satisfied. In addition to the hypothesis RH5, let the counterclockwise direction be positive for the absolute angle q_N , see Figure 15.

Let $(p_c^h, p_c^v)^\top$ be the Cartesian coordinates of the center of the mass and let $(p_a^h, p_a^v)^\top$ be the Cartesian coordinates of the stance ankle. Let $(p_{FRI}^h, 0)^\top$ be the FRI point on the ground and $\vec{F}_R = (0, F_R^N)^\top$ be the ground reaction force at the FRI point. Note that the tangential reaction force is zero by the definition of the FRI point. Let \vec{r}_1 be a vector from the stance toe to the center of mass, \vec{r}_2 represent the vector from the stance toe to stance ankle, and \vec{r}_3 denote the vector from the stance ankle to the center of mass, respectively. Let \vec{R} be the vector from the stance toe to the FRI point. Let Ψ denote the angle of \vec{r}_1 from horizontal and let ψ represent the angle between \vec{r}_1 and the stance foot. Then, $\Psi = q_N - \psi + q_{N,0}$, where $q_{N,0}$ is a constant such that the stance foot is on the

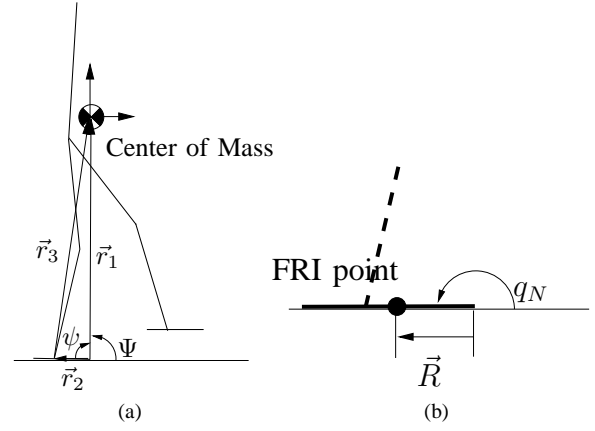


Fig. 15. Definition of parameters.

ground if $q_N = \pi - q_{N,0}$. The location of the center of mass can be written as

$$p_c^h = |\vec{r}_1| \cos(q_N - \psi + q_{N,0}) \quad (99)$$

$$p_c^v = |\vec{r}_1| \sin(q_N - \psi + q_{N,0}) \quad (100)$$

Note that $|\vec{r}_1|$ and ψ are independent of q_N due to the hypothesis RH5.

Let K and V be the kinetic energy and potential energy for the robot, respectively. Then, the potential energy of the robot is given as

$$V = mg|\vec{r}_1| \sin(q_N - \psi + q_{N,0}). \quad (101)$$

Define the Lagrangian as

$$L = K - V. \quad (102)$$

Using (99) and (101), the following is obtained.

$$\frac{\partial V}{\partial q_N} = mgp_c^h. \quad (103)$$

Therefore,

$$\frac{\partial L}{\partial q_N} = \frac{\partial K}{\partial q_N} - \frac{\partial V}{\partial q_N} = -\frac{\partial V}{\partial q_N} = -mgp_c^h, \quad (104)$$

since q_N is a cyclic variable so that $\partial K/\partial q_N = 0$.

By the property 1 in [36],

$$\frac{\partial L}{\partial \dot{q}_N} = \sigma_N, \quad (105)$$

where σ_N denotes the angular momentum about the stance toe. Since $\vec{r}_1 = \vec{r}_2 + \vec{r}_3$,

$$\sigma_N = \sigma_{N-1} + \vec{r}_2 \times mv_c, \quad (106)$$

where σ_{N-1} denotes the angular momentum about the stance ankle, v_c is the velocity of the center of mass, and $\vec{r}_2 = [p_a^h \ p_a^v]^\top$. Then, (105) and (106) imply

$$\frac{d}{dt} \frac{\partial L}{\partial \dot{q}_N} = \frac{d}{dt} (\sigma_{N-1} + \vec{r}_2 \times mv_c) = \dot{\sigma}_{N-1} + mp_a^h \ddot{p}_c^v - mp_a^v \ddot{p}_c^h. \quad (107)$$

Since there is no actuation at the stance toe, the only torque applied is from the ground reaction force. Using the method of Lagrange, the following is obtained.

$$\frac{d}{dt} \frac{\partial L}{\partial \dot{q}_N} - \frac{\partial L}{\partial q_N} = \vec{R} \times \vec{F}_R = p_{FRI}^h F_R^N, \quad (108)$$

which, together with (104) and (107), implies

$$\dot{\sigma}_{N-1} + mp_a^h \ddot{p}_c^v - mp_a^v \ddot{p}_c^h + mgp_c^h = p_{FRI}^h F_R^N. \quad (109)$$

Using (20) with the angular momentum balance theorem yields

$$-mg(p_c^h - p_a^h) + u_A + mp_a^h \ddot{p}_c^v - mp_a^v \ddot{p}_c^h + mgp_c^h = p_{FRI}^h F_R^N. \quad (110)$$

Therefore,

$$p_{FRI}^h F_R^N = mgp_a^h + mp_a^h \ddot{p}_c^v - mp_a^v \ddot{p}_c^h + u_A. \quad (111)$$

Since $F_R^N = mg + m\ddot{p}_c^v$, (111) yields the location of the FRI point as

$$p_{FRI}^h = p_a^h + \frac{-mp_a^v \ddot{p}_c^h + u_A}{F_R^N}. \quad (112)$$

ACKNOWLEDGMENT

The authors would like to thank Christine Chevallereau for helpful comments during the course of this work.

REFERENCES

- [1] R. R. Neptune, S. A. Kautz, and F. E. Zajac, "Contributions of the individual ankle plantar flexors to support, forward progression and swing initiation during walking," *Journal of Biomechanics*, vol. 34, pp. 1387–1398, 2001.
- [2] M. Meinders, A. Gitter, and J. M. Czerniecki, "The role of ankle plantar flexor muscle work during walking," *Scandinavian Journal of Rehabilitation Medicine*, vol. 30, pp. 39–46, 1998.
- [3] P. Saradin and G. Bessonnet, "Gait analysis of a human walker wearing robot feet as shoes," in *Proc. of the IEEE International Conference on Robotics and Automation, Seoul, Korea, May 2001*, pp. 2285–2292.
- [4] Honda Corp., ASIMO Website, 2005, <http://world.honda.com/ASIMO/>.
- [5] K. Hirai, M. Hirose, Y. Haikawa, and T. Takenaka, "The development of honda humanoid robot," in *Proceedings of the IEEE International Conference On Robotics and Automation, Leuven, Belgium, May 1998*, pp. 1321–1326.
- [6] Sony Corp., Qrio Website, 2005, <http://www.sony.net/SonyInfo/QRIO/>.
- [7] Johnnie - The TUM Biped Walking Robot, Website, 2005, <http://www.amm.mw.tu-muenchen.de/Misc/Messe/hanmesse-e.html>.
- [8] F. Pfeiffer, K. Löffler, and M. Gienger, "The concept of jogging johnnie," in *Proc. of the IEEE International Conference on Robotics and Automation, Washington, DC, May 2002*.
- [9] Y. Hurmuzlu, "Dynamics of bipedal gait - part 1: objective functions and the contact event of a planar five-link biped," *Journal of Applied Mechanics*, vol. 60, pp. 331–336, June 1993.
- [10] —, "Dynamics of bipedal gait - part 2: stability analysis of a planar five-link biped," *Journal of Applied Mechanics*, vol. 60, pp. 337–343, June 1993.
- [11] M. Spong, "Passivity based control of the compass gait biped," in *Proc. of IFAC World Congress, Beijing, China, July 1999*.
- [12] M. W. Spong and F. Bullo, "Controlled symmetries and passive walking," *IEEE Transactions on Automatic Control*, vol. 50, no. 7, pp. 1025–1031, 2005.
- [13] A. D. Kuo, "Energetics of actively powered locomotion using the simplest walking model," *Journal of Biomechanical Engineering*, vol. 124, pp. 113–120, 2002.
- [14] C.-L. Shih, "Ascending and descending stairs for a biped robot," *IEEE Transactions on Systems, Man, and Cybernetics*, 1999.
- [15] K. Y. Yi, "Walking of a biped robot with compliant ankle joints: implementation with kubca," in *Proc. of the 39th IEEE Conf. Dec. and Control, Sydney, Australia, December 2000*, pp. 4809–4814.
- [16] T. Takahashi and A. Kawamura, "Posture control for biped robot walk with foot toe and sole," in *27th Annual Conference of the IEEE Industrial Electronics Society*, 2001, pp. 329–334.
- [17] J. Park, "Impedance control for biped locomotion," *IEEE Transactions on Robotics and Automation*, 2001.
- [18] F. Silva and J. Tenreiro Machado, "Gait analysis of a human walker wearing robot feet as shoes," in *Proc. of the IEEE International Conference on Robotics and Automation, Seoul, Korea, May 2001*, pp. 4122–4127.
- [19] M. Morisawa, Y. Fujimoto, T. Murakami, and K. Ohnishi, "A walking pattern generation for a biped robot with parallel mechanism by considering contact force," in *27th Annual Conference of the IEEE Industrial Electronics Society*, 2001, pp. 2184–2189.
- [20] J. Grizzle, G. Abba, and F. Plestan, "Asymptotically stable walking for biped robots: Analysis via systems with impulse effects," *IEEE Transactions on Automatic Control*, vol. 46, pp. 51–64, January 2001.
- [21] E. Westervelt, J. Grizzle, and D. Koditschek, "Hybrid zero dynamics of planar biped walkers," *IEEE Transactions on Automatic Control*, vol. 48, no. 1, pp. 42–56, January 2003.
- [22] E. R. Westervelt, G. Buche, and J. W. Grizzle, "Experimental validation of a framework for the design of controllers that induce stable walking in planar bipeds," *International Journal of Robotics Research*, vol. 24, no. 6, pp. 559–582, June 2004.
- [23] C. Chevallereau, G. Abba, Y. Aoustin, E. Plestan, F. Westervelt, C. Canduas-de Wit, and J. Grizzle, "RABBIT: A testbed for advanced control theory," *IEEE Control Systems Magazine*, vol. 23, no. 5, pp. 57–79, October 2003.
- [24] E. Westervelt, J. Grizzle, and C. Canudas-de-Wit, "Switching and PI control of walking motions of planar biped walkers," *IEEE Transactions on Automatic Control*, vol. 48, no. 2, pp. 308–312, February 2003.
- [25] J. H. Choi and J. W. Grizzle, "Planar bipedal robot with foot rotation," in *American Control Conference, Portland, OR, June 2005*, pp. 4909–4916.
- [26] A. Goswami, "Postural stability of biped robots and the foot-rotation indicator (FRI) point," *International Journal of Robotics Research*, vol. 18, no. 6, pp. 523–533, June 1999.
- [27] F. Asano, M. Yamakita, N. Kamamichi, and Z.-W. Luo, "A novel gait generation for biped walking robots based on mechanical energy constraint," in *Proceedings of the IEEE/RSJ Conference On Intelligent Systems and Robots, Lausanne, Switzerland, October 2002*, pp. 2637–2644.
- [28] Y. Hurmuzlu and D. Marghitu, "Rigid body collisions of planar kinematic chains with multiple contact points," *International Journal of Robotics Research*, vol. 13, no. 1, pp. 82–92, 1994.
- [29] C. Chevallereau, E. R. Westervelt, and J. W. Grizzle, "Asymptotic stabilization of a five-link, four-actuator, planar bipedal runner," in *IEEE Conf. on Decision and Control, Atlantis, Paradise Island, Bahamas, December 2004*, pp. 303–310.
- [30] J. Guckenheimer and S. Johnson, "Planar hybrid systems," in *Hybrid Systems II, Lecture Notes in Computer Science*. Springer-Verlag, 1995, pp. 203–225.
- [31] J. H. Choi and J. W. Grizzle, "Planar bipedal robot with impulsive foot action," in *IEEE Conf. on Decision and Control, Paradise Island, Bahamas, December 2004*, pp. 296–302.
- [32] M. Vukobratović and B. Borovac, "Zero-moment point—thirty five years of its life," *International Journal of Humanoid Robotics*, vol. 1, no. 1, pp. 157–173, 2004.
- [33] M. Vukobratović, B. Borovac, D. Surla, and D. Stokic, *Biped Locomotion*. Berlin: Springer-Verlag, 1990.
- [34] K. Löffler, M. Gienger, and F. Pfeiffer, "Sensors and control concept of walking "johnnie"," *International Journal of Robotics Research*, vol. 22, no. 3-4, pp. 229–239, March-April 2003.
- [35] J. H. Choi, "Model-based control and analysis of anthropomorphic walking," Ph.D. dissertation, the University of Michigan, August 2005.
- [36] J. H. Choi and J. W. Grizzle, "Feedback control of an underactuated planar bipedal robot with impulsive foot action," *Robotica*, vol. 23, pp. 567–580, September 2005.